Check for updates

View Article Online
View Journal

RSC Sustainability

Accepted Manuscript

This article can be cited before page numbers have been issued, to do this please use: M. R. Hasan, S. Akter, S. Rabi, S. Majumder, R. Saha, M. A. R. Khan and A. K. Roy, *RSC Sustainability*, 2026, DOI: 10.1039/D6SU00189K.

This is an Accepted Manuscript, which has been through the Royal Society of Chemistry peer review process and has been accepted for publication.

Accepted Manuscripts are published online shortly after acceptance, before technical editing, formatting and proof reading. Using this free service, authors can make their results available to the community, in citable form, before we publish the edited article. We will replace this Accepted Manuscript with the edited and formatted Advance Article as soon as it is available.

You can find more information about Accepted Manuscripts in the Information for Authors.

Please note that technical editing may introduce minor changes to the text and/or graphics, which may alter content. The journal's standard Terms & Conditions and the Ethical guidelines still apply. In no event shall the Royal Society of Chemistry be held responsible for any errors or omissions in this Accepted Manuscript or any consequences arising from the use of any information it contains.

ROYAL SOCIETY OF CHEMISTRY

View Article Online
DOI: 10.1039/D6SU00189K

Sustainability spotlight:

The increasing demand for antimicrobial materials in healthcare, food industry, water treatment, and environmental remediation raises concerns over the environmental and health impacts of conventional fabrication methods using toxic chemicals and non-renewable resources. This work addresses these challenges by converting abundant agricultural waste (jute stick biomass) into nanocellulose (JNC) and integrating it with nitrogen-doped carbon quantum dots (N-CQDs) to form a functional substrate. Silver nanoparticles (AgNPs) are synthesized via UV irradiation, eliminating hazardous reducing agents. The resulting eco-friendly composite films exhibit high antibacterial efficiency and may support circular material design with potential biodegradability and scalability. This strategy aligns with UN Sustainable Development Goals 3, 6, 12, and 13 by combining waste-to-resource conversion, green synthesis, and multifunctional performance.

Open Access Article. Published on 24 June 2026. Downloaded on 6/25/2026 5:01:05 AM.
This article is licensed under a Creative Commons Attribution-NonCommercial 3.0 Unported Licence.

RSC Sustainability Accepted Manuscript

View Article Online
DOI: 10.1039/D6SU00189K

ARTICLE

Open Access Article. Published on 24 June 2026. Downloaded on 6/25/2026 5:01:05 AM.
This article is licensed under a Creative Commons Attribution-NonCommercial 3.0 Unported Licence.

UV-Light-Driven Fabrication of Antibacterial AgNPs-Decorated Nanocellulose/N-CQDs Free-Standing Composite Films

Received 00th January 20xx,
Accepted 00th January 20xx

DOI: 10.1039/x0xx00000x

Md Rakibul Hasan,[a] Selina Akter,[b] Saswata Rabi,[a] Sumit Majumder,[c] Ramkrishna Saha,[d] Md. Azizur R. Khan,[e] and Arup Kumer Roy*[a]

In this study, we present a sustainable and green approach for the fabrication of antibacterial free-standing films by incorporating silver nanoparticles (AgNPs) into a jute stick-derived nanocellulose and nitrogen-doped carbon quantum dots (N-CQDs) composite matrix via a UV-light-assisted process. Comprehensive characterization using XRD, FT–IR, FE-SEM, EDX, and XPS confirmed the successful synthesis and uniform deposition of AgNPs within the fluorescent nanocomposite matrix. The resulting films exhibited excellent antibacterial activity against *Klebsiella pneumoniae* (99.94% inhibition) and *Staphylococcus aureus* (99.99% inhibition). The demonstrated antibacterial efficacy, combined with the film's biodegradability and renewable substrate, highlights its potential for applications in antimicrobial packaging, water purification, and wound healing dressings. This work establishes a scalable and eco-friendly strategy for converting agricultural biomass into high-value functional nanomaterials.

Introduction

The growing concern of antibiotic-resistant bacteria has triggered an urgent global need for developing sustainable and environmentally friendly antibacterial materials. In recent years, significant research attention has focused on the development of multifunctional nanocomposite film materials that exhibit notable antibacterial activity, mechanical strength, and sustainability. Antibacterial films are considered highly effective in killing or inhibiting the growth of pathogenic microorganisms due to their high surface area and the efficient interaction of incorporated antimicrobial agents with bacterial cell membranes.[1,2] In this regard, multifunctional antibacterial films[3] have attracted increasing attention due to their potential applications in healthcare[4], water treatment[5], smart textiles[6] and the food industry.[7] Among the various sustainable material platforms developed to date, nanocellulose-based films have emerged as highly promising candidates due to their abundance, biodegradability, good mechanical properties, large surface area, and excellent film-forming capability.[8,9]

Nanocellulose (NC) is a promising green nanomaterial of the modern era. In previous studies, NC has been successfully extracted from a wide range of lignocellulosic biomass sources, including bamboo fibre,[10] sugarcane bagasse,[11] hemp stalks,[12] rice husks,[13] wastepaper,[14] filter paper,[15] and various other agricultural residues.[16] Among these resources, the woody core of the jute plant (*Corchorus* spp.), commonly known as jute sticks, represents a particularly promising yet underutilized source. Moreover, owing to its abundance, biodegradability, biocompatibility, and eco-friendliness, NC can be a promising platform for biomedical applications such as wound dressings, drug delivery systems, and related biomedical fields.[17]

In addition, carbon quantum dots (CQDs) have gained widespread interest due to their excellent photoluminescence properties, high quantum yield, water dispersibility, chemical inertness, and biocompatibility.[18,19] Typically, CQDs consist of an sp^2-hybridized carbon core decorated with numerous surface functional groups or heteroatom dopants. The most common functional groups present on the carbon core include hydroxyl (–OH), carboxyl (–COOH), carbonyl (–C=O), and amino ($–NH_2$) groups. Furthermore, various heteroatom dopants, such as nitrogen (N), sulphur (S), and phosphorus (P), can be incorporated into the CQD structure. These dopants possess lone-pair electrons or different electronegativity compared to carbon atoms, thereby enhancing the electron-donating capability of the CQDs.[20,21]

[a] Department of Chemistry, Chittagong University of Engineering and Technology, Chattogram-4349, Bangladesh.
[b] Department of Microbiology, Jashore University of Science and Technology, Jashore-7408, Bangladesh.
[c] Department of Biomedical Engineering, Chittagong University of Engineering and Technology, Chattogram-4349, Bangladesh.
[d] Department of Chemistry, Shahjalal University of Science and Technology, Sylhet-3114, Bangladesh.
[e] Department of Chemistry, Jashore University of Science and Technology, Jashore-7408, Bangladesh.

RSC Sustainability Accepted Manuscript

Open Access Article. Published on 24 June 2026. Downloaded on 6/25/2026 5:01:05 AM.
This article is licensed under a Creative Commons Attribution-NonCommercial 3.0 Unported Licence.

Among these, nitrogen doped quantum dots (N-CQDs) have attracted considerable attention within the scientific community because of their strong electron-donating ability toward metal ions.[22] N-CQDs are typically synthesized via bottom-up approaches, including hydrothermal and microwave-assisted methods, using nitrogen-rich precursors such as ethanolamine (EA),[23] urea,[24] ethylenediamine,[25] or the combination of citric acid-amine groups.[26] These nitrogen atoms are integrated into the carbon framework as pyridinic, pyrrolic, or graphitic forms,[27,28] which not only enhances their photoluminescence properties but also provides active sites for metal coordination and catalytic activity.[29]

In recent years, metallic nanoparticles (MNPs), such as silver (Ag), gold (Au), copper (Cu), and iron (Fe), have been extensively investigated for a wide range of applications owing to their unique physicochemical properties and potential antibacterial activity.[30] Among these MNPs, silver nanoparticles (AgNPs) have garnered significant attention in biomedical applications because of their exceptional antibacterial properties.[31] Conventionally, AgNPs are synthesized using chemical reducing agents such as sodium borohydride ($NaBH_4$),[32] hydrazine,[33] or trisodium citrate[34], which facilitate the reduction of Ag^+ ions to metallic silver (Ag^0). Although these methods are efficient, they often rely on hazardous chemical reducing agents and generate toxic by-products,[35] raising concerns about environmental impact and limiting their suitability for sustainable and biomedical applications.

To address this limitation, we introduce a facile and eco-friendly approach (**Fig. 1)** for synthesizing AgNPs using N-CQDs derived from EA and lemon as both reducing and stabilizing agents.[36,37] The abundant surface functional groups, including $–NH_2$, –OH, and –COOH, not only enable efficient electron transfer for the reduction of Ag^+ ions but also facilitate strong coordination with the resulting AgNPs.[38,39]

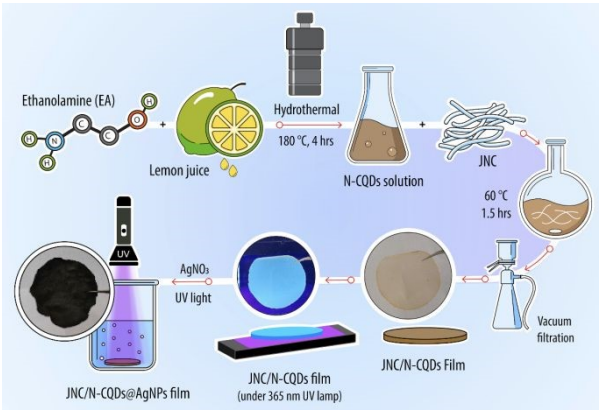

Fig. 1 Synthesis procedure of JNC/N-CQDs@AgNPs composite film.

The resulting composite films exhibited strong antibacterial activity against both Gram-positive (*S. aureus*) and Gram-negative (*K. pneumoniae*) bacteria. To the best of our knowledge, this study represents the first approach on the fabrication of AgNP-decorated N-CQD composite films using nanocellulose derived from jute sticks as the substrate.

Experimental details

View Article Online
DOI: 10.1039/D6SU00189K

Materials

Jute sticks and lemon were collected from a local market in Bangladesh. Sodium hydroxide (NaOH, Merck), sodium sulfite (Na_2SO_3, Smart Lab), sodium chlorite ($NaClO_2$, Loba Chemie), acetic acid (CH_3COOH, Merck), sodium acetate trihydrate ($CH_3COONa·3H_2O$, Merck), sulfuric acid (H_2SO_4, 98%, Merck), silver nitrate ($AgNO_3$, Merck), and EA (C_2H_7NO, Research Lab) were used in this study. Deionized (DI) water was used throughout all experiments. All chemicals were of analytical grade and used without further purification. UV light irradiation was performed using a 365 nm UV flashlight (UV Beast V3, USA).

Characterization

Fourier transform infrared (FT-IR) spectra were recorded using a PerkinElmer Spectrum FT-IR spectrometer (USA) in the range of 400–4000 cm^{-1} to analyze the chemical structure of the samples. Optical characterization was carried out using a PG Instruments T80+ UV–Vis spectrophotometer and a photoluminescence (PL) spectrophotometer (RF-5301 PC, Shimadzu). The surface morphology and elemental mapping were examined using field-emission scanning electron microscopy (FE-SEM, JEOL JSM-6010LA). The crystalline and amorphous structures of the samples were analyzed by X-ray diffraction (XRD) using a D/MAX 2500 V diffractometer (Rigaku SmartLab) with Cu Kα radiation (λ = 0.154 nm) operated at 40 kV and 30 mA over a 2θ range of 5°–80°. X-ray photoelectron spectroscopy (XPS) measurements were performed using a K-Alpha spectrometer (Thermo Fisher Scientific, USA) equipped with a hemispherical electron analyzer and micro-focused monochromatic Al Kα radiation.

Synthesis of nanocellulose from jute stick

Nanocellulose was extracted from jute sticks as described in the Supporting Information. For the preparation of jute-derived nanocellulose (JNC), 10 g of bleached jute stick (JS) cellulose was hydrolyzed with 87.5 mL of chilled 64 % H_2SO_4 at 45 °C for 30 min under magnetic stirring (400 rpm). After hydrolysis, the reaction was quenched by slowly pouring the mixture into a 2 L beaker containing cold deionized (DI) water and diluting the suspension to a final volume of 1 L. The diluted suspension was allowed to stand overnight. The mixture was then centrifuged at 7000 rpm for 20 min, and the supernatant containing the nanocellulose suspension was collected. Subsequently, the obtained suspension was dialyzed against DI water using a dialysis membrane (MWCO 1000 Da) for 3 days to remove residual H_2SO_4. Finally, the purified JNC suspension was stored at low temperature.

Preparation of N-CQDs/Nanocellulose film

For the preparation of N-CQDs, fresh lemon juice and EA were used in a 10:1 volume ratio (**Fig. 1)**, with lemon juice and EA serving as the carbon and nitrogen sources, respectively. Prior to synthesis, lemon juice was extracted by manual squeezing and filtered through a 0.22 µm membrane to remove pulp and

RSC Sustainability Accepted Manuscript

This journal is © The Royal Society of Chemistry 20xx

View Article Online
DOI: 10.1039/D6SU00189K

Open Access Article. Published on 24 June 2026. Downloaded on 6/25/2026 5:01:05 AM.
This article is licensed under a Creative Commons Attribution-NonCommercial 3.0 Unported Licence.

seeds. The filtrate was then centrifuged at 5000 rpm for 10 min to eliminate any residual particulates.

Subsequently, 60 mL of the lemon juice was mixed with 6 mL of EA under magnetic stirring for 30 min. The resulting mixture was transferred to a PPL-lined stainless-steel autoclave and subjected to hydrothermal treatment at 180 °C for 4 h. After cooling to room temperature, the brown N-CQD solution was collected and purified by dialysis using a 1000 Da molecular weight cut-off (MWCO) membrane (**Fig. S1a)**.

For composite film preparation, 15 mL of the purified N-CQD solution was mixed with 30 mL JNC solution and stirred at 60 °C for 90 min. The resulting dispersion was then filtered through a 0.22 µm nylon membrane using vacuum filtration. The brown-colored film was dried at 60 °C and carefully peeled from the membrane to obtain a free-standing fluorescent N-CQD–nanocellulose composite film (**Fig. S2a, b).**

Deposition of AgNPs onto JNC/N-CQD film

For the deposition of AgNPs, a 0.1 M $AgNO_3$ solution was prepared using deionized (DI) water. The previously prepared brown coloured fluorescent JNC/N-CQD film was immersed in the $AgNO_3$ solution and irradiated with UV light at 365 nm. Within 1–2 min, the film developed a deep reddish-brown color, indicating the successful formation of AgNPs on the surface of the N-CQD film. The AgNP-decorated film was then removed from the solution, rinsed several times with DI water to eliminate unreacted $AgNO_3$, and dried at room temperature (**Fig. S2c).**

Antimicrobial test

Method

Revival of bacterial culture

Gram-positive (*Staphylococcus aureus*, ATCC 25923) and Gram-negative (*Klebsiella pneumoniae*, ATCC 13883) strains were employed in this study. Frozen glycerol stock cultures were thawed and cultured overnight at 37 °C in Tryptic Soy Broth and MacConkey Broth, respectively. Following incubation, a loopful of each culture was streaked onto Mannitol Salt Agar plates (*S. aureus*) and MacConkey Agar plates (*K. pneumoniae*) to obtain isolated colonies for subsequent experiments.

Preparation of bacterial suspension

A single colony from a pure culture plate was transferred into 1 mL of sterile normal saline (0.85% NaCl). The resulting bacterial suspension was adjusted to a turbidity equivalent to the 0.5 McFarland standard (~1.5 × 10^8 CFU/mL) to ensure a standardized inoculum for reproducible antibacterial testing.[40]

Decontamination of the films

The synthesized films were trimmed to dimensions of 2.5 × 2.2 cm^2 and appropriately labelled. The films were placed on sterile glass Petri dishes and subjected to dry heat sterilization at 100 °C for 1 h prior to the antimicrobial experiments.

Retention of bacteria on the films

Using sterile tweezers, the films were immersed in bacterial suspensions prepared from overnight cultures and adjusted to the 0.5 McFarland standard. The films were then incubated for 30 min to allow bacterial adhesion to the film surface. To prevent desiccation, the films were then placed on sterile agar plates without nutrients. The films were then incubated at 37 °C for 18 h.

Serial dilution

After incubation, the films were removed from the agar plate and immersed in 10 mL of phosphate-buffered saline (PBS) and mixed thoroughly using a vortex mixer for 5 min. The film was then removed from buffered saline solution, and the resulting bacterial suspension was subjected to ten successive 10-fold serial dilutions in sterile PBS to determine the bacterial load on the film surfaces.

Drop plate technique

Following serial dilution, 10 µl drops from each dilution were dispensed onto the Mueller-Hinton Agar (MHA) and incubated at 37 °C for 18 h. Discrete colonies from each drop were counted, and the total bacterial load on the film was calculated by accounting for the average colony counts and dilution factors. The final bacterial count was expressed as colony-forming units per square centimeter of film (CFU cm^{-2}). Bacterial counts on treated films were compared to those on untreated control films, and the antimicrobial effect was expressed as the percentage reduction in bacterial numbers.

Calculation of bacterial loads

The bacterial reduction on the films was quantified using the following formulas:

$$\text{Percentage reduction} = \frac{C - T}{C} \times 100 \quad (1)$$

where C and T represent the colony-forming units (CFU cm^{-2}) on the control and treated films, respectively. The experiments were performed in triplicate (n = 3) to assess reproducibility, and the results are presented as mean ± standard deviation.

Results and discussion

Jute sticks, an abundantly available and renewable agricultural by-product, were utilized as a sustainable source for the production of nanocellulose, which serves as a biodegradable substrate. Prior to incorporation into this substrate, N-CQDs were synthesized through a green approach using EA as the nitrogen source[23] and lemon juice as a natural carbon precursor.[41] These N-CQDs contain abundant surface functional groups, such as –COOH, –OH, and $–NH_2$, which play a crucial role in the formation of AgNPs by facilitating the reduction of Ag^+ ions. In addition, these functional groups provide stabilization against the agglomeration of AgNPs on the JNC/N-CQDs surfaces.[39] Furthermore, the use of UV irradiation accelerates the reduction process, resulting in a significant decrease in the overall reaction time.[42]

RSC Sustainability Accepted Manuscript

View Article Online
DOI: 10.1039/D5SU00828K

Open Access Article. Published on 24 June 2026. Downloaded on 6/25/2026 5:01:05 AM.
This article is licensed under a Creative Commons Attribution-NonCommercial 3.0 Unported Licence.

RSC Sustainability Accepted Manuscript

Optical property analysis

The UV–Vis spectra of the as-prepared light-brown N-CQDs solution were investigated and are presented in **Fig. S1b.** The UV–Vis spectra exhibited a weak absorption band in the UV region at around 210 nm, which can be attributed to the π–π* electronic transition of aromatic sp^2-hybridized carbon (C=C) bonds. In addition, a shoulder peak appears at around 290 nm, arising from surface functional groups such as C=O, C–N, or –C–OH, present in the form of –COOH or $–NH_2$ groups on the surface of the N-CQDs.[43] Furthermore, the absorption tail extending into the visible region suggests the presence of surface defect states and surface-related energy levels within the carbon dot structure.[44] The photoluminescence (PL) spectra **(Fig. S1c)** exhibit a maximum excitation peak at 370 nm, with a corresponding emission peak at approximately 450 nm, resulting in blue fluorescence.

Structural analysis

The presence of various functional groups in the JNC, JNC/N-CQDs, and JNC/N-CQDs@AgNPs films was examined using ATR–FT–IR spectroscopy (**Fig. 2a**). The FT–IR spectrum of JNC displays prominent bands in the range of 1100–1000 cm^{-1}, which are attributed to C–O–C stretching vibrations and β-glycosidic bonds.[45] In addition, characteristic peaks are observed around 3400 cm^{-1} corresponding to O–H stretching vibrations and near 2900 cm^{-1} associated with C–H stretching.[46] After the incorporation of N-CQDs into the JNC matrix, two new peaks appear at approximately 1575 cm^{-1} and 1480 cm^{-1}, corresponding to N–H bending and C–N stretching vibrations, respectively, indicating the presence of amine groups derived from citric acid and EA.[47] Furthermore, a broad band observed near 3360 cm^{-1} is attributed to N–H stretching vibrations.[48] These spectral changes confirm the successful incorporation of N-CQDs within the JNC matrix.

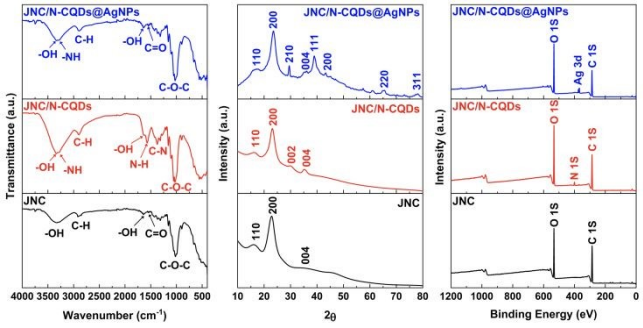

Fig. 2 Comparative Structural Analysis of JNC, JNC/N-CQDs and JNC/N-CQDs@AgNPs by (a) ATR-FT–IR and (b) XRD (c) XPS.

For the JNC/N-CQDs@AgNPs film, a noticeable reduction in the intensity of the $–NH_2$ and –OH bands is observed, which can be attributed to their involvement in the reduction of Ag^+ ions to metallic AgNPs.[38] This observation suggests the successful formation of the JNC/N-CQDs@AgNPs composite film.

As shown in **Fig. 2b**, the XRD pattern of JNC exhibits three characteristic diffraction peaks at 2θ ≈ 15°, 22.5° and a relatively broad peak of lower intensity around 34.8° , which correspond to the (110), (200), and (004) crystallographic planes of nanocellulose, respectively.[49] After the incorporation of N-CQDs, a new diffraction peak appears at approximately 27.7° (002) due to the graphitic carbon. The broad nature of this peak indicates the largely amorphous or poorly crystalline structure of the N-CQDs.[50,51]

For the JNC/N-CQDs@AgNPs composite film, additional diffraction peaks are observed at 2θ ≈ 27.8°, 38.1°, 44.3°, 46.2°, 64.4°, and 77.4°, corresponding to the (210), (111), (200), (231), (220), and (311) planes of metallic silver, respectively.[52,53] These peaks confirm the successful formation and crystalline nature of AgNPs within the composite film.

To gain deeper insight into the surface chemical composition and elemental states of the three samples, X-ray photoelectron spectroscopy (XPS) analysis was performed. As shown in **Fig. 2c**, the survey spectra of all samples confirm the presence of carbon (C 1s), nitrogen (N 1s), and oxygen (O 1s) at binding energies of approximately 285, 400, and 532 eV, respectively. In addition, two characteristic silver peaks corresponding to Ag $3d_5/_2$ and Ag $3d_3/_2$ are observed in the range of 368–374 eV, confirming the presence of silver in the JNC/N-CQDs@AgNPs composite film.[54]

The deconvoluted C 1s spectrum of all samples (**Fig. 3a**) showed three primary components corresponding to C-C/C=C (~284.2 eV), C-O (~285.8 eV), C=O (~287.8 eV), bonds, respectively.[55] After the incorporation of N-CQDs, the relative intensity of the oxygen-containing carbon functional groups (C–O and C=O) increased noticeably, with a peak observed near ~286.3 eV, accompanied by a relative decrease in the C–C/C=C component. This change indicates the successful incorporation of oxygen-rich N-CQDs onto the JNC surface.

As expected, no N 1s signal was detected in the pristine JNC sample. However, after the incorporation of N-CQDs, a distinct N 1s peak appeared (**Fig. 2c**). The deconvoluted N 1s spectrum of the JNC/N-CQDs sample exhibits three characteristic components attributed to pyridinic N (~398.8 eV), N–H (~400.1 eV), and graphitic N (~400.8 eV) (**Fig. S3**).[20]

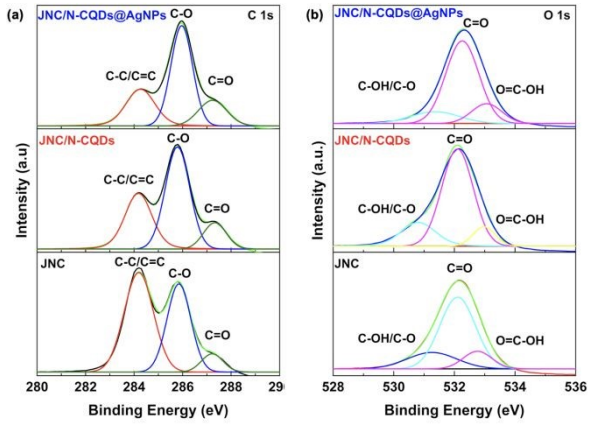

Fig. 3 XPS spectra of comparison deconvoluted peaks of (a) C 1s, and (b) O 1s for JNC, JNC/N-CQDs and JNC/N-CQDs@AgNPs.

In the high-resolution Ag 3d spectrum, two well-defined peaks corresponding to Ag $3d_5/_2$ and Ag $3d_3/_2$ are observed at approximately 368.8 and 374.8 eV, respectively (**Fig. 4**),

This journal is © The Royal Society of Chemistry 20xx

View Article Online
DOI: 10.1039/D6SU00180H

Open Access Article. Published on 24 June 2026. Downloaded on 6/25/2026 5:01:05 AM.
This article is licensed under a Creative Commons Attribution-NonCommercial 3.0 Unported Licence.

confirming the formation of AgNPs on the surface of the JNC/N-CQDs film.[56]

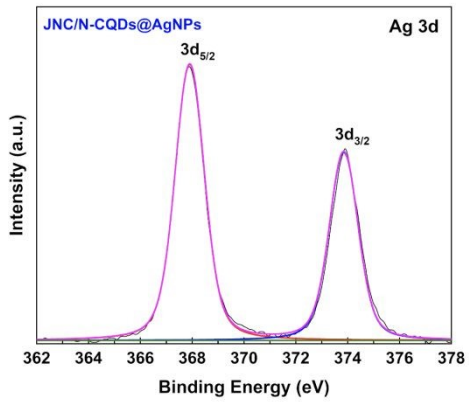

Fig. 4 High-resolution Ag 3d spectrum of the JNC/N-CQDs@AgNPs nanocomposite film.

Upon the incorporation of AgNPs, a noticeable decrease in the intensity of the N 1s peak around 400.2 eV (**Fig. 2c**) is observed, suggesting that nitrogen-containing functional groups participate as electron donors during the reduction of Ag^{+} to metallic Ag^{0}.[57,58] This interpretation is further supported by the deconvoluted N 1s spectrum (**Fig. S3**), which is consistent with the results obtained from FT-IR and EDX analyses.

For all samples, the O 1s spectra (**Fig. 3b**) exhibit three distinct peaks at approximately 531.5, 532.4 and 533.1 eV, which are attributed to C-OH/C-O, C=O and O=C-OH groups, respectively.[59]

Surface morphology

The surface morphology of the prepared films was examined using field-emission scanning electron microscopy (FE-SEM), as shown in **Fig. 5** and **Fig. S4**. The pristine JNC sample in **Fig. S4a** exhibits a fibrous and entangled network structure composed of relatively uniform and smooth fibrils. The individual cellulose fibres display a smooth surface with widths ranging from approximately 0.8 to 2.5 µm. The microfibrils are clearly distinguishable and form a porous interconnected network, providing a high surface area that is favourable for subsequent functionalization.

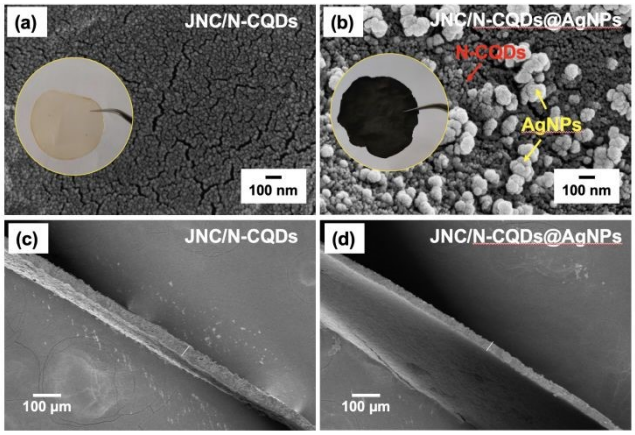

Fig. 5 FE-SEM images of (a) JNC/N-CQDs (b) JNC/N-CQDs@AgNPs and cross-sectional images of (c) JNC/N-CQDs (d) JNC/N-CQDs@AgNPs.

After the incorporation of N-CQDs into the JNC matrix (**Fig. 5a**), the film surface becomes noticeably rougher, with dispersed granular or dot-like features distributed throughout the fibrillar network. It can further be observed that the N-CQDs are relatively uniform and densely distributed, with particle sizes estimated to be approximately 10–20 nm. The N-CQDs are likely anchored onto the JNC matrix through hydrogen-bonding and/or electrostatic interactions between the functional groups present on both components.

As observed in **Fig. 5b**, the surface is densely covered with uniformly distributed spherical AgNPs. The high particle density and relatively consistent size of the AgNPs indicate a successful in situ reduction process facilitated by N-CQDs under UV irradiation (365 nm) within a short reaction time. In this process, the N-CQDs act as both reducing and stabilizing agents, promoting homogeneous nucleation and preventing nanoparticle agglomeration.

Cross-sectional SEM images (**Fig. 5c**, **d**) confirmed the formation of continuous films with relatively uniform thickness. The JNC/N-CQDs film exhibited a comparatively less compact structure with an average thickness of approximately 46.61 ± 1.27 µm, whereas the JNC/N-CQDs@AgNPs film showed a denser and slightly thinner cross-sectional profile with a thickness of about 37.33 ± 0.52 µm. This difference may be attributed to the incorporation and aggregation of AgNPs within the film matrix.

The energy-dispersive X-ray (EDX) spectra obtained from FE-SEM (**Fig. S5**) reveal that the final composite film is dominated by AgNPs (85.69%), indicating that the N-CQDs effectively reduced Ag^{+} ions and facilitated their deposition on the JNC/N-CQDs surface. In addition, the relative atomic percentages of C, O, and N decrease markedly compared with JNC and JNC/N-CQDs after the formation of AgNPs. These observations are further supported by the elemental mapping images of the composite film (**Fig. S6**), which show prominent signals corresponding to Ag (Ag Lα1) along with C (C Kα1), O (O Kα1), and N (N Kα1,2), confirming the uniform distribution of AgNPs within the JNC/N-CQDs matrix.

Table 1: Comparison of bacterial loads between control and treated films.

Strain	Samples	Count	Reduction
		log $CFUcm^{-2}$	(C-T)/C × 100
S. aureus	JNC (C)	8.70 ± 0.33	-
	N-CQDs (T)	7.55 ± 0.29	92.92 ± 0.99
	JNC/N-CQDs@AgNPs (T)	3.73 ± 0.19	99.99 ± 0.00
K. pneumoniae	JNC (C)	7.24 ± 0.39	-
	N-CQDs (T)	6.54 ± 0.43	79.82 ± 2.25
	JNC/N-CQDs@AgNPs (T)	3.95 ± 0.07	99.94 ± 0.03

C= Control film, T=Treated film

Antibacterial performance

To evaluate antibacterial performance, all experiments were performed in triplicate (n = 3), and the results are presented (**Table 1**) as mean ± standard deviation (SD). Percentage reduction values were calculated based on the mean bacterial counts using the control reference.

RSC Sustainability Accepted Manuscript

View Article Online
DOI: 10.1039/D6SU00189H

Open Access Article. Published on 24 June 2026. Downloaded on 6/25/2026 5:01:05 AM.
This article is licensed under a Creative Commons Attribution-NonCommercial 3.0 Unported Licence.

For *S. aureus*, the bacterial adhesion assay revealed clear differences among the samples. The control JNC film exhibited a bacterial load of 8.70 ± 0.33 log CFU cm^{-2}, whereas the N-CQDs-incorporated film and the JNC/N-CQDs@AgNPs composite showed significantly lower counts of 7.55 ± 0.29 log CFU cm^{-2} and 3.73 ± 0.19 log CFU cm^{-2}, respectively. These values correspond to bacterial reductions of approximately 93% for the N-CQDs-incorporated film and 99.9% for the JNC/N-CQDs@AgNPs composite relative to the control, demonstrating the composite's strong antibacterial activity and its substantially enhanced ability to inhibit bacterial adhesion compared with both the pristine JNC and the N-CQDs-incorporated film.

Furthermore, for *K. pneumoniae*, a pronounced reduction in bacterial load was observed on the modified films compared with the control JNC film. The control JNC film exhibited a bacterial load of 7.24 ± 0.39 log CFU cm^{-2}, whereas the N-CQDs-incorporated film showed a markedly lower value of 6.54 ± 0.43 log CFU cm^{-2}. For the JNC/N-CQDs@AgNPs composite, the bacterial count was 3.95 ± 0.07 log CFU cm^{-2}. These results confirm that the modified films, particularly the JNC/N-CQDs@AgNPs composite, exhibit strong antibacterial activity against *K. pneumoniae*.

The superior antibacterial performance of the JNC/N-CQDs@AgNPs composite can be attributed to multiple complementary mechanisms. The incorporation of N-CQDs facilitates uniform dispersion and stabilization of AgNPs within the nanocellulose matrix. This prevents aggregation and maximizes the effective surface area available for antimicrobial interactions. The well-dispersed AgNPs enable sustained release of Ag^+ ions, which interact with thiol (-SH) groups in proteins, causing enzyme inactivation and disruption of essential metabolic pathways.[60]

Additionally, AgNPs induce the generation of reactive oxygen species (ROS), leading to oxidative stress, lipid peroxidation, and nucleic acid damage.[61] Moreover, N-CQDs may facilitate electron transfer, further enhancing ROS generation and amplifying antibacterial activity.[62,63] Additionally, direct contact between nanoparticles and bacterial membranes can result in physical disruption, increasing membrane permeability and causing leakage of intracellular contents.[64]

The difference in antibacterial efficacy between *S. aureus* (Gram-positive) and *K. pneumoniae* (Gram-negative) can be explained by their distinct cell envelope architectures. Gram-negative bacteria possess an outer lipopolysaccharide (LPS) membrane and a relatively thin peptidoglycan layer. This structure may allow more efficient penetration of Ag^+ ions and nanoparticles. In contrast, Gram-positive bacteria have a thick, highly cross-linked peptidoglycan layer, which acts as a protective barrier, thereby limiting nanoparticle diffusion and reducing susceptibility.[65] This structural difference likely accounts for the lower reduction in bacterial count observed for *S. aureus* compared to *K. pneumoniae*. Additionally, electrostatic interactions between the negatively charged bacterial surfaces and the functional groups on N-CQDs and AgNPs may further influence bacterial adhesion and antimicrobial efficiency.[66]

In addition to antibacterial activity, the composite film also exhibits anti-adhesive characteristics. The incorporation of nanocellulose and N-CQDs may influence the surface roughness, hydrophilicity, and surface charge of the film.[67] A more hydrophilic and negatively charged surface can reduce initial bacterial adhesion by minimizing favorable interactions with bacterial cell walls.[68] Consequently, the observed reduction in CFU counts likely arises from the combined effects of inhibited bacterial adhesion and enhanced bactericidal activity.

The strong antibacterial performance of the JNC/N-CQDs@AgNPs composite, particularly against Gram-negative bacteria, highlights its potential in applications such as biomedical coatings, wound dressings, food packaging, and water purification systems. The extremely low bacterial counts, often below the detection limit, demonstrate effective bacterial inhibition under the tested conditions.

The developed JNC/N-CQDs@AgNPs film exhibited antibacterial performance comparable to or exceeding that reported for several previously reported biopolymer-based AgNP composite films (**Table 2**). The film exhibited approximately 99.9% inhibition against both *K. pneumoniae* and *S. aureus*, demonstrating strong broad-spectrum antibacterial activity. In comparison, earlier studies based on chitosan (CHI),[69] starch,[70] carrageenan (CG),[71] polylactic acid (PLA),[72] and konjac glucomannan (KGM) matrices[73] generally reported lower inhibition efficiencies or smaller inhibition zones.[73] Direct quantitative comparisons among different studies should, however, be interpreted with caution, as antibacterial performance can be influenced by factors such as bacterial strain, testing methodology, and experimental conditions.

In addition to the incorporation of AgNPs, the present work employs a hybrid structure comprising N-CQDs and AgNPs within a JNC matrix to enhance antibacterial performance. Another important advantage is the use of jute stick biomass as an environmentally friendly, renewable source of nanocellulose, offering a sustainable and potentially cost-effective alternative to synthetic or commercially available polymer-based substrates. Furthermore, the UV-light-assisted synthesis method provides a rapid and environmentally friendly route for AgNP formation without the use of conventional chemical reducing agents. These integrated features position the composite film as a promising candidate for applications including wound dressings, antibacterial coatings, and food packaging materials.

However, despite these advantages, this study possesses certain limitations. In particular, the toxicity, biocompatibility, and mechanical durability of the developed composite films were not directly evaluated. While nanocellulose is generally recognized as biocompatible and biodegradable,[74,75] and N-CQDs typically exhibit low cytotoxicity,[76] the potential cytotoxic effects associated with AgNPs warrant careful consideration. Although their *in-situ* formation and immobilization within the JNC/N-CQDs matrix may help reduce direct exposure and modulate Ag^+ release,[77] systematic experimental validation is still required.

RSC Sustainability Accepted Manuscript

View Article Online
DOI: 10.1039/D6SU00189K

ARTICLE

Open Access Article. Published on 24 June 2026. Downloaded on 6/25/2026 5:01:05 AM.
This article is licensed under a Creative Commons Attribution-NonCommercial 3.0 Unported Licence.

Table 2. Comparison of the present work with previously reported antibacterial based materials.

Ref.	Film	Substrate/Polymer	Reducing Agent	Antibacterial Performance
[78]	CHI/EOs/AgNPs	CHI	Tyrosine	3.4 log CFU g^{-1} (*E. coli), 6.3* log CFU g^{-1} *(L. monocytogenes), 2.7* log CFU g^{-1} *(S. Typhimurium)*
[69]	CHI-AgNPs/Glycerol	CHI	Sucrose	21.9 ± 0.5 mm (*E. coli*), 17.6 ± 0.6 mm (*B. subtilis*)
[70]	bio-AgNPs	Starch + PBAT	*Fusarium oxysporum*	10^5-10^6 CFU cm^{-2} (*E. coli, S. aureus*, and *S. Typhimurium*)
[73]	KGM/SA/N-CQD	KGM + SA	-	99.2% (S. *putrefaciens)*, 98.99% (*S. aureus)*
[72]	PLA/MPE/AgNPs	PLA	MPE	95% (*E. coli,* and *S. aureus*)
[79]	SSPS/AgNPs	SSPS	SSPS	4.1 ± 0.3 (*E. coli),* 3.5 ± 0.2 mm (*S. aureus*)
[71]	SSPS/CG/AgNP	CG	SSPS	1.92 ± 0.25 mm (*E. coli*), 1.83 ± 0.13 mm (*S. aureus*)
This work	JNC/N-CQDs@AgNPs	JNC	N-CQDs under UV light	~99.9% inhibition (*K. pneumoniae,* and *S. aureus*)

CG: Carrageenan; CHI: Chitosan; EOs: Essential oil; KGM: Konjac glucomannan; MPE: Mango peel extract; PBAT: Poly (butylene adipate co-terephthalate); PLA: Polylactic acid; SA: Sodium alginate; SSPS: Soluble soybean polysaccharide.

Conclusions

In this work, we present a facile, sustainable, and green strategy for fabricating antibacterial free-standing films via the in-situ incorporation of AgNPs within a composite of JNC and N-CQDs using a UV-light-assisted process. The nitrogen-rich functional groups in the JNC/N-CQDs network act as electron donors, enabling Ag^+ reduction, while UV irradiation accelerates nanoparticle formation, ensuring uniform and well-dispersed AgNPs throughout the matrix.

Comprehensive physicochemical characterization (FT-IR, XRD, XPS, FE-SEM, and EDX) confirms the successful integration of AgNPs into the fluorescent nanocomposite framework without compromising structural integrity. The resulting films exhibit excellent antibacterial performance, achieving ~99.9% reduction against *S. aureus* and *K. pneumoniae*, demonstrating both bacteriostatic and bactericidal effects.

The enhanced antimicrobial efficacy of the films is attributed to improved surface interactions, possible reactive oxygen species (ROS) generation, and sustained Ag^+ release arising from the synergistic interaction between the nanocellulose scaffold, N-CQDs, and uniformly dispersed AgNPs. The pronounced activity against both Gram-positive and Gram-negative bacteria highlights the composite's broad-spectrum antibacterial potential.

This work therefore presents an eco-friendly and potentially scalable platform for developing multifunctional antibacterial materials from renewable biomass. Although the composite film exhibits strong antibacterial activity, comparative evaluations involving JNC/AgNP and AgNP-only systems would help quantify the individual contributions of AgNPs and N-CQDs and further reveal potential synergistic antibacterial effects within the composite film.

Furthermore, the toxicity and biocompatibility of the developed composite were not directly evaluated in this study, providing an important direction for future validation toward biomedical and practical applications. Nanocellulose is generally considered biocompatible and biodegradable, while N-CQDs typically exhibit low cytotoxicity. In addition, although AgNPs may exhibit concentration-dependent cytotoxic effects, their *in-situ* formation and immobilization within the JNC/N-CQDs matrix are expected to reduce direct exposure and help regulate Ag^+ release. Nevertheless, further systematic studies on film stability, controlled Ag^+ release, and comprehensive biocompatibility assessment are required for translation into practical applications.

Complementary investigations, including rigorous statistical analysis of antimicrobial performance across different bacterial strains and conditions, comprehensive mechanical characterization under processing and operational stresses, *in vitro* and *in vivo* cytotoxicity evaluation, and detailed investigation of antibacterial mechanisms, are essential prior to adoption of the material for applications such as wound dressings, food packaging, and antimicrobial coatings.

Author contributions

Md Rakibul Hasan: Conceptualization, Data curation, Methodology, Visualization, Original draft; **Selina Akter:** Analysis, Data curation, Visualization, Original draft; **Saswata Rabi:** Analysis, Data curation, Visualization, Project administration; **Sumit Majumder:** Conceptualization, Data curation, Visualization, Writing - review & editing; **Ramkrishna Saha:** Analysis, Data curation, Visualization; **Md. Azizur R. Khan:** Analysis, Data curation, Visualization; **Arup Kumer Roy:** Conceptualization, Methodology, Project administration, Supervision, Visualization, Analysis, Writing - review & editing.

Conflicts of interest

There are no conflicts to declare.

RSC Sustainability Accepted Manuscript

View Article Online
DOI: 10.1039/D6SU00189K

Data availability

The data supporting this study are provided in the Supplementary Information (SI). The SI includes the experimental procedure for the preparation of jute stick–derived cellulose, along with representative images and the UV–Vis and photoluminescence (PL) spectra of the N-CQDs solution. In addition, EDX analyses of the JNC, JNC/N-CQDs, and JNC/N-CQDs@AgNPs films are presented. The SI further contains the deconvoluted N 1s XPS spectra of the JNC/N-CQDs and JNC/N-CQDs@AgNPs samples, as well as FE-SEM images with corresponding elemental color mapping of the JNC/N-CQDs@AgNPs film.

Acknowledgements

This research was carried out with the support of the Advanced Research in Education Grants Program (PS20222088), funded by the Bangladesh Bureau of Educational Information and Statistics (BANBEIS) under the Ministry of Education, Government of the People's Republic of Bangladesh.

References

1 S. Ippili, J. S. Jung, A. M. Thomas, V. H. Vuong, J. M. Lee, M. S. Sha, K. K. Sadasivuni, V. Jella and S. G. Yoon, *Polymers (Basel).*, DOI:10.3390/polym15183791.
2 K. Singh, S. Prakash, D. Choudhury, D. S. Jayas, M. Kumari, R. K. Singh, R. Koundal and A. K. Chauhan, *Food Control*, DOI:10.1016/j.foodcont.2025.111855.
3 B. F. Finina and A. K. Mersha, *RSC Adv.*, 2024, **14**, 5290–5308.
4 Y. Liang, Y. Liang, H. Zhang and B. Guo, *Asian J. Pharm. Sci.*, 2022, **17**, 353–384.
5 L. Zhang, X. Bai, H. Tian, L. Zhong, C. Ma, Y. Zhou, S. Chen and D. Li, *Carbohydr. Polym.*, 2012, **89**, 1060–1066.
6 S. Majumder, A. K. Roy, W. Jiang, T. Mondal and M. J. Deen, *IEEE J. Flex. Electron.*, 2023, **3**, 120–150.
7 E. J. Jang, B. Padhan, M. Patel, J. K. Pandey, B. Xu and R. Patel, *Food Control*, DOI:10.1016/j.foodcont.2023.109902.
8 I. Elfaleh, F. Abbassi, M. Habibi, F. Ahmad, M. Guedri, M. Nasri and C. Garnier, *Results Eng.*, DOI:10.1016/j.rineng.2023.101271.
9 H. Kargarzadeh, J. Huang, N. Lin, I. Ahmad, M. Mariano, A. Dufresne, S. Thomas and A. Gałęski, *Prog. Polym. Sci.*, 2018, **87**, 197–227.
10 H. Singh, A. K. Verma, A. K. Trivedi and M. K. Gupta, *Mater. Today Proc.*, 2022, **106**, 1–6.
11 K. S. Mohammed, M. Atlabachew, B. Abdu and A. A. Desalew, *Sci. Rep.*, DOI:10.1038/s41598-024-81403-0.
12 X. Zhang, J. Guo, Y. Liu, X. Hao, Q. Yao, Y. Xu and Y. Guo, *J. Mater. Chem. B*, DOI:10.1039/d3tb00440f.
13 N. Samsalee, J. Meerasri and R. Sothornvit, *Carbohydr. Polym. Technol. Appl.*, DOI:10.1016/j.carpta.2023.100353.
14 R. Goswami, A. Mishra, A. Mirza, W. Ahmad and R. Rana, *J. Appl. Polym. Sci.*, DOI:10.1002/app.56275.
15 Z. Wang, W. Zhang, J. Yu, L. Zhang, L. Liu, X. Zhou, C. Huang and Y. Fan, *Cellulose*, 2019, **26**, 1183–1194.
16 M. C. Alvarado, M. C. C. D. Ignacio, M. C. G. Acabal, A. R. P. Lapuz and K. F. Yaptenco, *Nano Trends*, DOI:10.1016/j.nwnano.2024.100054.
17 J. Li, R. Cha, K. Mou, X. Zhao, K. Long, H. Luo, F. Zhou and X. Jiang, *Adv. Healthc. Mater.*, DOI:10.1002/adhm.201800334.
18 L. Cui, X. Ren, M. Sun, H. Liu and L. Xia, *Nanomaterials*, DOI:10.3390/nano11123419.
19 A. K. Roy, W. Ghann, S. Rabi, J. Barua, S. Majumder, R. Amin, M. K. M. Ziaul Hyder and J. Uddin, *RSC Sustain.*, 2024, **2**, 1003–1013.
20 K. G. Nguyen, I. A. Baragau, R. Gromicova, A. Nicolaev, S. A. J. Thomson, A. Rennie, N. P. Power, M. T. Sajjad and S. Kellici, *Sci. Rep.*, DOI:10.1038/s41598-022-16893-x.
21 S. D. Dsouza, M. Buerkle, P. Brunet, C. Maddi, D. B. Padmanaban, A. Morelli, A. F. Payam, P. Maguire, D. Mariotti and V. Svrcek, *Carbon N. Y.*, 2021, **183**, 1–11.
22 P. Wu, W. Li, Q. Wu, Y. Liu and S. Liu, *RSC Adv.*, 2017, **7**, 44144–44153.
23 X. Dong, Y. Su, H. Geng, Z. Li, C. Yang, X. Li and Y. Zhang, *J. Mater. Chem. C*, 2014, **2**, 7477–7481.
24 S. Kumar M, Y. Y. K, P. Das, S. Malik, N. K. Kothurkar and S. K. Batabyal, *J. Sci. Adv. Mater. Devices*, DOI:10.1016/j.jsamd.2021.11.005.
25 H. Qi, Z. Zhai, X. Dong and P. Zhang, *Spectrochim. Acta - Part A Mol. Biomol. Spectrosc.*, DOI:10.1016/j.saa.2022.121456.
26 S. Kostromin, A. Borodina, D. Pankin, A. Povolotskiy and S. Bronnikov, *Chem. Phys. Lett.*, DOI:10.1016/j.cplett.2024.141175.
27 A. Pramanik, S. Biswas, C. S. Tiwary, R. Sarkar and P. Kumbhakar, *ACS Omega*, 2018, **3**, 16260–16270.
28 R. Hu, L. Li and W. J. Jin, *Carbon N. Y.*, 2017, **111**, 133–141.
29 X. Wang, Y. Feng, P. Dong and J. Huang, *Front. Chem.*, DOI:10.3389/fchem.2019.00671.
30 A. Girma, G. Mebratie, B. Mekuye, B. Abera, T. Bekele and G. Alamnie, *Nano Sel.*, DOI:10.1002/nano.202400049.
31 S. Raza, M. Wdowiak, M. Grotek, W. Adamkiewicz, K. Nikiforow, P. Mente and J. Paczesny, *Nanoscale Adv.*, 2023, **5**, 5786–5798.
32 U. T. Khatoon, A. Velidandi and G. V. S. Nageswara Rao, *Mater. Chem. Phys.*, DOI:10.1016/j.matchemphys.2022.126997.
33 V. Gurusamy, R. Krishnamoorthy, B. Gopal, V. Veeraravagan and Periyasamy, *Inorg. Nano-Metal Chem.*, 2017, **47**, 761–767.
34 M. S. Arif, R. Ulfiya, Erwin and A. S. Panggabean, *AIP Conf. Proc.*, DOI:10.1063/5.0059493.
35 K. R. Hakeem, M. Kamli, J. S. M. Sabir and H. F. Alharby, *Divers. Appl. Nanotechnol. Biol. Sci.*, DOI:10.1201/9781003277255.
36 M. Meltsner, C. Wohlberg and M. J. Kleiner, *J. Am. Chem. Soc.*, 1935, **57**, 2554.
37 M. Mahiuddin and B. Ochiai, *ACS Omega*, 2022, **7**, 35626–35634.

Open Access Article. Published on 24 June 2026. Downloaded on 6/25/2026 5:01:05 AM.
This article is licensed under a Creative Commons Attribution-NonCommercial 3.0 Unported Licence.
RSC Sustainability Accepted Manuscript

View Article Online
DOI: 10.1039/D5SU00189K

38 L. Shen, M. Chen, L. Hu, X. Chen and J. Wang, *Langmuir*, 2013, **29**, 16135–16140.
39 A. K. Roy, S. M. Kim, P. Paoprasert, S. Y. Park and I. In, *RSC Adv.*, 2015, **5**, 31677–31682.
40 M. K. Lalitha, *Indian Assoc. Med. Microbiol.*, 2007, 1–47.
41 M. He, J. Zhang, H. Wang, Y. Kong, Y. Xiao and W. Xu, *Nanoscale Res. Lett.*, DOI:10.1186/s11671-018-2581-7.
42 F. Chutrakulwong, K. Thamaphat and M. Intarasawang, *Nanomaterials*, DOI:10.3390/nano14121018.
43 A. Tadesse, M. Hagos, D. Ramadevi, K. Basavaiah and N. Belachew, *ACS Omega*, 2020, **5**, 3889–3898.
44 Z. Kang and S. T. Lee, *Nanoscale*, 2019, **11**, 19214–19224.
45 J. Huang, M. Ma, M. Qin, X. Li and Y. Ren, *Int. J. Mol. Sci.*, DOI:10.3390/ijms262010222.
46 C. Aumnate, N. Soatthiyanon, T. Makmoon and P. Potiyaraj, *Cellulose*, 2021, **28**, 8509–8525.
47 A. Kundu, B. Maity and S. Basu, *ACS Omega*, 2023, **8**, 22178–22189.
48 W. D. Yang, C. Y. Liu, Z. Y. Zhang, Y. Liu and S. D. Nie, *J. Mater. Chem.*, 2012, **22**, 23012–23016.
49 O. Somseemee, P. Saeoui, F. T. Schevenels and C. Siriwong, *Sci. Rep.*, DOI:10.1038/s41598-022-10558-5.
50 H. A. S. Tohamy, *Emergent Mater.*, 2025, **8**, 2425–2437.
51 A. Aygun, N. Bennini, R. N. E. Tiri, I. Kaynak and F. Sen, *Next Nanotechnol.*, DOI:10.1016/j.nxnano.2025.100150.
52 R. I. Priyadharshini, G. Prasannaraj, N. Geetha and P. Venkatachalam, *Appl. Biochem. Biotechnol.*, 2014, **174**, 2777–2790.
53 Y. Meng, *Nanomaterials*, 2015, **5**, 1124–1135.
54 C. Correia, J. Martinho and E. Maçôas, *Nanomaterials*, DOI:10.3390/nano12030385.
55 Q. Li, Z. Guo, X. Zhao, T. Zhang, J. Chen and Y. Wei, *Nanotechnology*, DOI:10.1088/1361-6528/ab8f4b.
56 J. Yan, B. Zhang, L. Guo and Z. Wang, *J. Phys. Chem. C*, 2019, **123**, 575–583.
57 S. Liu, B. Yu and T. Zhang, *RSC Adv.*, 2014, **4**, 544–548.
58 Y. Su, B. Shi, S. Liao, J. Zhao, L. Chen and S. Zhao, *ACS Sustain. Chem. Eng.*, 2016, **4**, 1728–1735.
59 K. Chang, Q. Zhu, L. Qi, M. Guo, W. Gao and Q. Gao, *Materials (Basel).*, DOI:10.3390/ma15020466.
60 E. O. Mikhailova, *J. Funct. Biomater.*, DOI:10.3390/jfb11040084.
61 H. M. Ali, K. Karam, T. Khan, S. Wahab, S. Ullah and M. Sadiq, *3 Biotech*, DOI:10.1007/s13205-023-03835-1.
62 F. Shen, Z. Lu, K. Yan, K. Luo, S. Pei and P. Xiang, *Sci. Rep.*, DOI:10.1038/s41598-025-14383-4.
63 DOI:10.1039/D6MA00039H.
64 S. Hayat, A. Ashraf, M. H. Siddique, B. Aslam, H. Shafaqat, S. Javed, Z. Taj, M. H. Sarfraz, H. Rafiq and S. Muzammil, *RSC Adv.*, 2025, **15**, 42460–42478.
65 B. Punz, C. Christ, A. Waldl, S. Li, Y. Liu, L. Johnson, V. Auer, O. Cardozo, P. M. A. Farias, A. C. D. S. Andrade, A. Stingl, G. Wang, Y. Li and M. Himly, *Environ. Sci. Nano*, 2025, **12**, 1710–1739.
66 C. Zhang, Y. Zheng, X. Lin and S. Weng, *RSC Adv.*, 2025, **15**, 22180–22201.
67 D. Thapliyal, G. D. Verros and R. K. Arya, *Polymers (Basel).*, DOI:10.3390/polym17020247.
68 S. Zheng, M. Bawazir, A. Dhall, H. E. Kim, L. He, J. Heo and G. Hwang, *Front. Bioeng. Biotechnol.*, DOI:10.3389/fbioe.2021.643722.
69 S. J. Santosa, M. Hadi, A. D. Hatmanto, S. M. Darmanastri, E. Kusrini, K. D. Nugrahaningtyas and A. Usman, *JCIS Open*, DOI:10.1016/j.jciso.2025.100155.
70 M. da S. das Neves, S. Scandorieiro, G. N. Pereira, J. M. Ribeiro, A. B. Seabra, A. P. Dias, F. Yamashita, C. B. do. R. Martinez, R. K. T. Kobayashi and G. Nakazato, *Antibiotics*, DOI:10.3390/antibiotics12010178.
71 J. Liu, Y. Dong, Z. Ma, Z. Rao, X. Zheng and K. Tang, *ACS Appl. Polym. Mater.*, 2022, **4**, 5608–5618.
72 J. Cheng, X. Lin, X. Wu, Q. Liu, S. Wan and Y. Zhang, *Int. J. Biol. Macromol.*, 2021, **188**, 678–688.
73 Z. Jiang, J. Feng, Y. Dai, W. Yu, S. Bai, C. Bai, Z. Tu, P. Guo, T. Liao and L. Qiu, *Int. J. Biol. Macromol.*, DOI:10.1016/j.ijbiomac.2025.139596.
74 C. Zinge and B. Kandasubramanian, *Eur. Polym. J.*, DOI:10.1016/j.eurpolymj.2020.109758.
75 K. Malekpour, A. Hazrati, A. Khosrojerdi, L. Roshangar and M. Ahmadi, *Regen. Ther.*, 2023, **24**, 630–641.
76 V. Singh, S. Kashyap, U. Yadav, A. Srivastava, A. V. Singh, R. K. Singh, S. K. Singh and P. S. Saxena, *Toxicol. Res. (Camb).*, 2019, **8**, 395–406.
77 J. U. Shin, J. Gwon, S. Y. Lee and H. S. Yoo, *ACS Omega*, 2018, **3**, 16150–16157.
78 S. Shankar, D. Khodaei and M. Lacroix, *Food Hydrocoll.*, DOI:10.1016/j.foodhyd.2021.106750.
79 J. Liu, Z. Ma, Y. Liu, X. Zheng, Y. Pei and K. Tang, *Food Packag. Shelf Life*, DOI:10.1016/j.fpsl.2021.100800.

Open Access Article. Published on 24 June 2026. Downloaded on 6/25/2026 5:01:05 AM.
This article is licensed under a Creative Commons Attribution-NonCommercial 3.0 Unported Licence.

RSC Sustainability Accepted Manuscript

View Article Online
DOI: 10.1039/D6SU00189K

Data availability

The data supporting this study are provided in the Supplementary Information (SI). The SI includes the experimental procedure for the preparation of jute stick–derived cellulose, along with representative images and the UV–Vis and photoluminescence (PL) spectra of the N-CQDs solution. In addition, energy-dispersive X-ray (EDX) analyses of the JNC, JNC/N-CQDs, and JNC/N-CQDs@AgNPs films are presented. The SI further contains the deconvoluted N 1s XPS spectra of the JNC/N-CQDs and JNC/N-CQDs@AgNPs samples, as well as FE-SEM images with corresponding elemental color mapping of the JNC/N-CQDs@AgNPs film.

Open Access Article. Published on 24 June 2026. Downloaded on 6/25/2026 5:01:05 AM.
This article is licensed under a Creative Commons Attribution-NonCommercial 3.0 Unported Licence.

RSC Sustainability Accepted Manuscript